Published in final edited form as:
J Am Chem Soc. 2009 December 23; 131(50): 18119–18128. doi:10.1021/ja904726q.

The Distal Pocket Histidine Residue in Horse Heart Myoglobin Directs the *O*-Binding Mode of Nitrite to the Heme Iron

Jun Yi[†], **Julie Heinecke**[‡], **Hui Tan**[†], **Peter C. Ford**[‡,*], and **George B. Richter-Addo**[†,*]

[†]Department of Chemistry and Biochemistry, University of Oklahoma, 620 Parrington Oval, Norman, OK 73019

[‡]Department of Chemistry and Biochemistry, University of California at Santa Barbara, Santa Barbara, CA 93106

Abstract

It is now well established that mammalian heme proteins are reactive with various nitrogen oxide species and that these reactions may play significant roles in mammalian physiology. For example the ferrous heme protein myoglobin (Mb) has been shown to reduce nitrite (NO_2^-) to nitric oxide (NO) under hypoxic conditions. We demonstrate here that the distal pocket histidine residue (His64) of horse heart metMb^{III} (i.e., ferric Mb^{III}) has marked effects on the mode of nitrite ion coordination to the iron center. X-ray crystal structures were determined for the mutant proteins metMb^{III} H64V (2.0 Å resolution) and its nitrite ion adduct metMb^{III} H64V-nitrite (1.95 Å resolution), and metMb^{III} H64V/V67R (1.9 Å resolution) and its nitrite ion adduct metMb^{III} H64V/V67R-nitrite (2.0 Å resolution). These are compared to the known structures of wild type hh metMb^{III} and its nitrite ion adduct hh metMb^{III}-nitrite, which binds NO_2^- via an O-atom in a *trans*-FeONO configuration. Unlike wt metMb^{III}, no axial H_2O is evident in either of the metMb^{III} mutant structures. In the ferric H64V-nitrite structure, replacement of the distal His residue with Val alters the binding mode of nitrite from the nitrito (*O*-binding) form in the wild-type protein to a weakly bound nitro (*N*-binding) form. Reintroducing a H-bonding residue in the H64V/V67R double mutant restores the *O*-binding mode of nitrite. We have also examined the effects of these mutations on reactivities of the metMb^{III}s with cysteine as a reducing agent and of the (ferrous) Mb^{II}s with nitrite ion under anaerobic conditions. The Mb^{II}s were generated by reduction of the Mb^{III} precursors in a second order reaction with cysteine, the rate constants for this step following the order H64V/V67R > H64V >> wt. The rate constants for the oxidation of the Mb^{II}s by nitrite (giving NO as the other product) follow the order wt > H64V/V67R >> H64V and suggest a significant role of the distal pocket H-bonding residue in nitrite reduction.

Introduction

The reduction of nitrite (NO_2^-; pK_a 3.2 at 20 °C)[1] to nitric oxide (NO) by denitrifying metalloenzymes is an important component of the global nitrogen cycle (eq. 1).[2–5]

$$NO_2^- + 2H^+ + 1e^- \rightarrow NO + H_2O \quad (1)$$

Such nitrite reduction by the heme-containing nitrite reductase (NiR) enzymes is generally believed to be preceded by the direct binding of nitrite anion to the heme iron centers in these proteins. Historically, biological nitrite reduction to NO has been primarily associated with

ford@chem.ucsb.edu, grichteraddo@ou.edu.

denitrifying bacteria. However, it is now known that certain mammalian tissues contain metalloproteins that reduce nitrite to NO.[6–10] The relevance of these mammalian proteins to physiological hypoxic NO production that circumvents the O_2-dependent NO synthase pathway is currently being debated. Hendgen-Cotta et al have, however, demonstrated that nitrite protects against myocardial infarction in $Mb^{+/+}$ mice, but does not in $Mb^{-/-}$ knockout mice, thus implicating Mb as an in vivo NiR.[11]

The nitrite anion binds to bacterial heme-containing NiRs via the *N*-binding "nitro" mode (Fig. 1, left).[12, 13] In contrast, we recently showed that nitrite binds to the ferric centers of horse heart myoglobin (hh Mb^{III})14 and human Hb[15] not through this nitro mode, but rather through the rather unusual (for heme proteins) *O*-binding "nitrite" mode (Fig. 1, middle). There is an alternative *O,O*-bidentate binding mode (Fig. 1, right), seen in the copper-containing NiRs from *Alcaligenes xylosoxidans* (the H313G mutant)[16] and *Achromobacter cycloclastes*,[17] but this has not yet been observed for any heme protein.

A key question is: What controls the *O*-binding mode of nitrite to the mammalian protein Mb? We hypothesized that the single H-bonding His64 distal pocket residue in hh Mb^{III} directs the nitrite ligand towards this *O*-binding mode and influences any subsequent nitrite reduction kinetics. In this context, we speculated that removing this His64 residue (e.g., the H64V mutant; Fig. 2) should allow the nitrite ligand to adopt the nitro *N*-binding mode, thus altering the rate of nitrite reduction, and that reintroducing a single H-bonding distal pocket residue (e.g., the H64V/V67R double mutant) could restore *O*-binding and reactivity. In this article, we report our findings on the structures of these systems and describe some of the chemical reactivity consequences of such mutations.

Materials and Methods

Materials

The plasmid of horse heart Mb H64V was a kind gift from Dr. Grant A. Mauk (University of British Columbia, Canada). The site-directed mutagenesis method was employed for preparation of the hh Mb H64V/V67R mutant using pGYM-H64V as the DNA template. The hh Mb H64V and H64V/V64R mutant proteins were expressed and purified according to the published method of Guillemette et al.[18] EDTA, DTPA, 3,4-dihydroxybenzoic acid, and Sephadex G-25 were purchased from Aldrich. Sodium nitrite (≥99.5%) was purchased from Fluka, and protocatechuate 3,4 dioxygenase was purchased from Sigma.

Crystallization

Crystals of the proteins were grown by the hanging drop vapor diffusion method at room temperature (~22 °C).

hh Mb^{III} H64V—A hanging drop containing an equal volume of 15 mg/mL protein solution and well solution was suspended over wells containing 2.8–3.3 M phosphate and 1 mM EDTA with pH from 6.4 to 7.2. The crystals appeared within one week in the drops containing 3.1–3.3 M phosphate at pH 6.4. Suitable sized crystals were harvested using cryo-loops and soaked in artificial mother liquor containing 10% glycerol as a cryoprotectant. The crystals were then flash-frozen in liquid nitrogen prior to data collection.

hh Mb^{III} H64V nitrite adduct—The hanging drops contained an equal volume of (i) 15 mg/mL protein solution in the presence of excess sodium nitrite and (ii) well solution. The drop was suspended over wells containing 2.8–3.3 M phosphate and 1 mM EDTA with pH from 6.4 to 7.2. The crystals appeared after one month in the drops containing 3.1–3.3 M phosphate at pH 6.4. Suitable sized crystals were harvested by cryo-loops and soaked in artificial mother

liquor containing 10% glycerol as a cryoprotectant. The crystals were then flash-frozen in liquid nitrogen prior to data collection.

hh Mb^{III} H64V/V67R—A hanging drop containing equal volume of 30 mg/mL protein solution and well solution was suspended over wells containing 2.8–3.3 M phosphate and 1 mM EDTA with pH from 6.4 to 7.2. The crystals appeared within one week in the drops containing 3.1–3.3 M phosphate at pH 6.4. Suitable sized crystals were harvested using cryo-loops and soaked in artificial mother liquor containing 10% glycerol as a cryoprotectant. The crystals were then flash-frozen in liquid nitrogen prior to data collection.

hh Mb^{III} H64V/V67R nitrite adduct—Crystals of hh Mb^{III} H64V/V67R were soaked in artificial mother liquor containing 25 mM sodium nitrite and 10% glycerol as a cryoprotectant. The crystals was soaked with nitrite for one day and then flash-frozen in liquid nitrogen prior to data collection.

X-ray Data Collection and Processing

X-ray diffraction data for crystals of the hh Mb^{III} H64V and hh Mb^{III} H64V/V67R mutants were collected at 104 K on a RigakuMSC RU-H3R X-ray generator (Moore laboratory, OUHSC) operated at 50 kV/100 mA to produce Cu/Kα radiation (λ= 1.5418 Å). For the hh Mb^{III} H64V crystal, 1° oscillation images were collected over a range of 197° with an exposure time of 7 min per image and a crystal-to-detector distance of 120 mm. For the hh Mb^{III} H64V/V67R crystal, 1° oscillation images were collected over a range of 200° with an exposure time of 7 min per image and a crystal-to-detector distance of 120 mm.

X-ray diffraction data for the hh Mb^{III} H64V nitrite and hh Mb^{III} H64V/V67R nitrite complexes were collected at 100 K on a RigakuMSC RU-H3R X-ray generator operated at 48 kV/98 mA to produce Cu/Kα radiation (λ= 1.5418 Å). For the hh Mb^{III} H64V nitrite crystal, 1° oscillation images were collected over a range of 190° with an exposure time of 6 min per image and a crystal-to-detector distance of 110 mm. For the hh Mb^{III} H64V/V67R nitrite crystal, 1° oscillation images were collected over a range of 210° with an exposure time of 5 min per image and a crystal-to-detector distance of 105 mm. All data sets were collected and processed using the stand-alone d*TREK program (Macintosh v.99D) from Molecular Structure Corporation.[19]

Structure Solution and Refinement

The phase information for the structures were obtained using the molecular replacement method as implemented in *PHASER* (v1.3.3).[20] A non-standard space group $P2_122_1$ suggested by the program *PHASER* was not recognized by the refinement software *REFMAC5*[21] as implemented in CCP4 (v6.0.2).[22] The *SFTOOL*, as implemented in CCP4 (v6.0.2), was used to manually change the header information from $P2_122_1$ to a standard space group $P2_12_12$, followed by a process of re-indexing reflections. The model was refined using *REFMAC5*. For the nitrite complexes, the Fe–(nitrite) bond distance and angle parameters were unrestrained throughout the refinement; however, internal restraints of 1.25(2) Å (for d(N-O)) and 119(3)° (for ∠ONO) were applied to the nitrite groups. *COOT* was used for visualization and model building/correction between refinement cycles.[23] The water molecules were added into all four structures using *ARP/wARP*[24] as implemented in CCP4. After completion of the refinement process, the interactive macromolecular structure validation tool *MolPROBITY* (available online from the Richardson Lab at Duke University at http://molprobity.biochem.duke.edu/) was utilized to assign the final rotamer orientations of Asn, Gln, and His sidechains, and to test for any unusual sidechain contacts.[25]

hh Mb^{III} H64V—The hh Mb^{III} H64V protein crystallizes with one molecule in the asymmetric unit, and the final model of its structure contains 153 amino acid residues, one heme group, one sodium cation, and 112 water molecules. One phosphate anion was modeled in the crystallographic lattice with 70% occupancy. The crystallographic R and R_{free} for the final model are 18.6% and 23.7%, respectively, in the 21.4–2.0 Å range.

hh Mb^{III} H64V nitrite complex—The hh Mb^{III} H64V nitrite complex crystallizes with one molecule in the asymmetric unit, and the final model of its structure contains 153 amino acid residues, one heme group, and 122 water molecules. Two nitrite anions were modeled in the structure. One was modeled in the active site with 65% occupancy and the other nitrite anion was modeled in the crystallographic lattice with full occupancy. A water molecule in the active site (labeled wat1) was modeled at 70% occupancy, and a second water molecule (labeled wat2) was modeled with a full occupancy. The crystallographic R and R_{free} for the final model are 19.8% and 25.0%, respectively, in the 23.2–1.95 Å range.

hh Mb^{III} H64V/V67R—The hh Mb^{III} H64V/V67R protein crystallizes with one molecule in the asymmetric unit, and the final model of its structure contains 153 amino acid residues, one heme group, and 153 water molecules. One phosphate anion was modeled in the crystallographic lattice with 60% occupancy. The crystallographic R and R_{free} for the final model are 18.0% and 23.3%, respectively, in the 24.4–1.90 Å range.

hh Mb^{III} H64V/V67R nitrite complex—The hh Mb^{III} H64V/V67R nitrite complex crystallizes with one molecule in the asymmetric unit, and the final model of its structure contains 153 amino acid residues, one heme group, and 92 water molecules. Three nitrite anions were modeled in the final structure. One was modeled in the active site with 65% occupancy, and the other two were in the crystallographic lattice with full occupancies. The sidechain of the Arg67 was modeled 65% occupancy due to disorder of the sidechain. One water molecule at full occupancy was modeled at the active site close to the protein surface; this water molecule H-bonds to the guanylyl group from the Arg67 residue. The crystallographic R and R_{free} for the final model are 20.2% and 25.8%, respectively, in the 20.6–2.0 Å range.

The crystal data are shown in Table 1. The $2F_o-F_c$ and F_o-F_c maps were generated using *FFT*) as implemented in CCP4. Figures were drawn using PyMOL (http://www.pymol.org) [26] and labels were added using Adobe®Photoshop.

Kinetics of Mb^{III} Reductions by Cysteine

All reactions were run under pseudo first order conditions in anaerobic, 25 °C, pH 7.41 phosphate buffer (100 mM) solutions containing 0.1 mM EDTA to chelate adventitious metal ions. The reaction kinetics were followed by recording the temporal absorbance changes using a Shimadzu Model UV2401-PC spectrophotometer. The protein concentrations were typically ~3–4 μM.

The cysteine reductions were initiated by using a gastight syringe to add deaerated stock solutions of cysteine to deaerated solutions of the proteins to give the final concentrations noted above and the desired cysteine concentration (1.0 mM in most cases). The temporal absorption changes were then recorded. These reactions followed simple (pseudo) first order decays from which k_{obs} values could be determined. For consistency, an initial rates method was used to determine the rate constants reported in this article; however, second order rate constants determined from the k_{obs} values were essentially the same.

Kinetics of Mb^{II} Oxidations by Nitrite

The nitrite reductase (NiR) activities of the reduced proteins were studied by using a gastight syringe to add deaerated stock solutions of sodium nitrite to product solutions of the cysteine reaction once completed. In most cases this gave an initial nitrite concentration of 1.0 mM as well as a cysteine concentration of 1.0 mM.

Dithionite (5 mM) was also used to reduce the ferric wt and mutant proteins. In the case where excess reductant (cysteine or dithionite) was removed before Mb^{II} oxidation, the solution was run over a G-25 Sephadex column. For these reactions, protocatechuate dioxygenase (0.05 μ/mL) was used with its substrate 3,4 dihydroxybenzoic acid (1 mM) to consume any adventitious O_2 and avoid protein autoxidation.[28] Sodium nitrite was then added as described for the systems with cysteine still present.

Results

We reported previously that the nitrite anion binds to wt $metMb^{III}$ via the η^1-O binding nitrito mode.[14] We now report our X-ray crystal structural determinations of the nitrite adduct of the single mutant $metMb^{III}$ H64V that does not possess a distal pocket H-bonding residue, and the structural determinations of the nitrite adduct of the double-mutant H64V/V67R that has an Arg residue that can reintroduce H-bonding capacity to the distal pocket. We also report the cysteine reduction of the $metMb^{III}$ derivatives and the rates of nitrite reduction by the wt Mb^{II} and the ferrous mutants.

The hh $metMb^{III}$ H64V Single Mutant Complexed with Nitrite

Addition of nitrite to $metMb^{III}$ H64V in phosphate buffer resulted in a small blue shift of the Soret band from 395 nm to 392 nm. This blue shift is in an opposite direction to that observed when nitrite is added to wt $metMb^{III}$ to form the Mb^{III}-nitrite adduct; in this latter case, the Soret band shifts from 409 nm to 412 nm.[29] In the Q band regions there was a decrease in the band at 500 nm and an increase at 572 nm. Suitable crystals of the nitrite adduct of the $metMb^{III}$ H64V mutant for an X-ray structural determination grew after one month using the hanging-drop method, and the crystal structure at 100 K was obtained at 1.95 Å resolution. A superposition of the C_α chains of the wt $metMb^{III}$ and the H64V mutant gives an average rmsd of 0.8 Å; the largest rmsds are in the GH loop region on the surface of the protein away from the heme site, namely for the residues His119-Pro120-Gly121-Asp122 with rmsds that range from 2.0–4.8 Å. In any event, the general α-helical fold of the protein is very similar to that for wt $metMb^{III}$ and will not be discussed further.

The $2F_o-F_c$ electron density map and F_o-F_c omit map of the heme site of this H64V nitrite adduct is shown in Figs. 3A and 3B together with the final crystallographic model. The F_o-F_c omit map clearly reveals the presence of new electron density in the distal pocket. The nitrite ligand was modeled into this electron density and refines best in the *N*-binding mode at 65% occupancy. The axial (His93)N–Fe–N(nitrite) bond angle is near linear at 177°.

The Fe–N(nitrite) bond distance of 2.6 Å is rather long and suggests that the nitrite ligand is held in the distal pocket by an electrostatic interaction with the ferric center. This is consistent with the observation that there is no continuous electron density from the Fe center to the nitrite ligand when the $2F_o-F_c$ electron density map is contoured at 1σ (Fig. 3A). When contoured at 0.9σ, however, continuous electron density linking these groups becomes evident (not shown). Such relatively weak binding of the NO_2^- suggests that the nitrite anion would be only weakly activated upon coordination to the ferric center of this H64V mutant in the absence of distal pocket H-bonding residues. Indeed, the bound nitrite is stabilized in the hydrophobic distal pocket by a water channel from the exterior of the protein as evidenced by a H_2O molecule (wat1 in Figs. 3A & B, that is best modeled at 70% occupancy) with a (nitrite)O…O(wat1)

distance of 2.9 Å. This wat1 molecule is further H-bonded to a second H_2O molecule (wat2; full occupancy) close to the surface of the protein with a (wat1)O…O(wat2) distance of 3.0 Å and a (wat2)O…O(nearest heme propionate) distance of 3.3 Å.

Experimental evidence for linkage isomerization of the nitrite ligand to the iron center has not been reported for any heme protein. The observation here of an *N*-bound nitrite in a Mb^{III} mutant when the wt Mb^{III} derivative displays *O*-binding preference is thus unprecedented. To help understand the likely origin of the weak binding of nitrite in the H64V adduct, we determined the X-ray crystal structure of the ferric H64V mutant without added nitrite. The H64V mutant has been widely used to study distal pocket H-bonding effects in Mbs,[30,31] and the structure of the related sperm whale $metMb^{III}$ H64V mutant is known.[32,33] However, the crystal structure of the hh $metMb^{III}$ H64V mutant has not been reported. We therefore similarly obtained its crystal structure at 2.0 Å resolution. The electron density maps do not show the presence of electron density that can be assigned to a fixed H_2O molecule bound to the ferric center. In contrast, the reported X-ray crystal structure of the analogous sw ferric H64V mutant at 110 K shows a bound H_2O molecule to Fe with a long Fe–O(water) bond distance of 2.4 Å.[32] In this latter low temperature sw H64V structure, the bound H_2O ligand (modeled at 50% occupancy) was held in place by a water channel similar to that observed in our hh Mb^{III} H64V nitrite structure. We conclude, therefore, that the nitrite ligand in the hh H64V nitrite complex is indeed only weakly bound to the ferric center, and that the general structure of the protein does not change significantly upon nitrite binding (an average rmsd of 0.2 Å is obtained when the C_α chains of the ferric H64V and the nitrite adduct are compared).

The hh Mb^{III} H64V/V67R Double Mutant Complexed with Nitrite

When $NaNO_2$ was added to a solution of Mb^{III} H64V/V67R, changes in the absorption spectrum in the Q band region were similar to those observed with the single mutant and wt metMb; there was a decrease at 500 nm and an increase in a band at 574 nm. We obtained X-ray diffraction-quality crystals of the nitrite adduct of the H64V/V67R double mutant by soaking crystals of the ferric precursor with sodium nitrite solution. The crystal structure of this adduct in the $P2_12_12$ space group was determined to 2.0 Å resolution. The $2F_o-F_c$ electron density map and F_o-F_c omit map of the heme site are shown in Figs. 4A and 4B. The maps clearly show electron density in the distal pocket due to the bound nitrite that was best modeled at 65% occupancy. The nitrite ligand is bound to the ferric center via the *O*-binding nitrito mode, with an Fe–O bond distance of 2.1 Å. Notably, the FeONO moiety in this double-mutant H64V/V67R complex is best modeled with a distorted *cis*-like conformation (Fig. 5) similar to that observed for the FeONO moiety in the β subunit of human *R*-state $Hb^{III}ONO$,[15] in contrast to the wt $Mb^{III}(ONO)$ complex where the nitrite is modeled in the *trans*-FeONO conformation. Furthermore, for the double mutant, the NO_2^- ligand is H-bonded to the distal Arg67 residue with an (Fe)O…N(Arg67) distance of 3.2 Å indicative of a moderate-to-weak H-bond.

The 2.0 Å resolution structure of the ferric H64V/V67R mutant without added nitrite is shown in Figs. 4C and 4D. As with the ferric H64V protein, no electron density is observed in the $2F_o-F_c$ map for an H_2O axially bound to the ferric center. Further, the Arg67 side-chain points out towards the solvent in this precursor compound.

A comparison of the structure of the nitrite adduct of the H64V/V67R double mutant with the structure of the ferric protein without nitrite reveals three very interesting structural consequences of nitrite binding to this protein, and these are illustrated in Fig. 6. First, upon nitrite binding, the Arg67 side-chain points inward to H-bond with the O1 atom of the nitrite ligand. Such a movement of a distal pocket Arg residue to H-bond with axially-bound ligands such as cyanide has been observed in its complex with Mb^{III} from the Mediterranean mollusc *Aplysia limacina* which contains a natural "H64V/V67R" configuration.[34] Second, the

swinging in of the Arg67 side-chain likely creates a steric conflict with a propionate (initially pointing up) in the precursor crystal that is relieved by a change in conformation to point downwards towards the proximal side of the heme. In doing so, however, the side-chain of the proximal (but non-Fe bound) His97 residue adopts a new position with its imidazole C_γ atom moving 2.9 Å from its initial position; thus, this His97 residue loses its initial H-bonding interaction with a propionate group. Indeed, the largest rmsds (avg of 0.2 Å) when the C_α chains of the ferric H64V/V67R and the nitrite adduct are compared are for the Lys96 (rmsd 1.3 Å) and the His97 (rmsd 1.1 Å) residues located at the end of the F-helix which suggests a partial unwinding of this region. Third, these motions result in a saddled heme group in the nitrite adduct that further distorts by bending towards the proximal side. Such movements upon binding a ligand are indeed remarkable given that these occurred after soaking nitrite into pre-formed crystals of the ferric H64V/V67R double mutant (Fig. 4C), and this reveals the flexibility of the heme environment even in this $P2_12_12$ crystal.

Reduction of the Mb^{III}s by Cysteine

Various reducing agents such as dithionite, ascorbate, and NADH have been used to reduce $metMb^{III}$s to their Mb^{II} derivatives.[35–39] However, the use of these reducing agents when nitrite is present has been shown to be problematic, as the reducing agents may react directly with nitrite.[35] Furthermore, using an excess of dithionite may have deleterious effects on the heme proteins.[36, 39, 40]

We find that cysteine ($E°$ (*RSSR/RSH*) = −245 mV)[41] is an effective, mild reducing agent for the clean generation of the ferrous myoglobins and, while being a more biologically relevant reductant than dithionite, it does not react with nitrite under our reaction conditions. To the best of our knowledge, this is the first report of the use of cysteine to reduce ferric heme proteins to their ferrous derivatives.

Anaerobic addition of excess cysteine to a solution of wt $metMb^{III}$ in phosphate buffer at pH 7.41 results in the slow absorbance decrease of the Soret band at 408 nm due to the $metMb^{III}$ and the concomitant appearance of a new Soret band at 433 nm (Fig. 7A). These spectral changes are accompanied by decreases in the Q bands of $metMb^{III}$ at 500 and 630 nm and appearance of a new band at 557 nm consistent with reduction of the wt $metMb^{III}$ to the $deoxyMb^{II}$ form. The rate of the reduction of the wt $metMb^{III}$ in this manner is first order in the concentrations of protein and of cysteine, and the second order rate constant k_2 for this reaction, determined by the initial rates method, is 0.069 M^{-1} s^{-1} at 25 °C.

The spectral changes that result from addition of excess cysteine to the ferric H64V single mutant (Fig. 7B) are also consistent with the reduction of the protein to its ferrous derivative. In this case, the second order rate constant is 0.60 $M^{-1}s^{-1}$, which is an order of magnitude larger than that measured for the wt protein. The faster rate is consistent with the more positive reduction potential of the H64V mutant ($E°$ = 87 mV) relative to the wt $metMb^{III}$ ($E°$ = 61 mV).[42] The spectral changes accompanying reduction of the H64V/V67R double mutant are shown in Fig. 7C, and the k_2 for cysteine reduction was determined to be 2.3 M^{-1} s^{-1}.

Overall, therefore, the second order rate constants for the reduction of the ferric wt and mutant proteins follow the order H64V/V67R > H64V >> wt. Importantly, the ferrous proteins were stable in the presence of excess cysteine, thus allowing for the follow-up reactions with nitrite to be carried out in the presence or absence of excess cysteine.

Nitrite Reduction by the Ferrous wt and Mutant Proteins

The rates of nitrite reduction by the wt and mutant $deoxyMb^{II}$s were measured by monitoring the disappearance of the absorption bands due to the $deoxyMb^{II}$s. The general sequence of

reactions involved may be defined by Scheme 1, and we use wt deoxyMb^{II} as an example to illustrate the nitrite reduction reaction. In earlier studies,[11] it was shown that addition of excess nitrite to a buffered solution of wt deoxyMb^{II} leads to the formation of a mixture of the ferrous nitrosyl Mb^{II}(NO) and metMb^{III}. These products were rationalized in terms of the proton assisted nitrite oxidation of deoxyMb^{II} to give the ferric nitrosyl complex Mb^{III}(NO) (the first step shown in Scheme 1). The latter is labile to NO dissociation,[43] and any NO released is rapidly scavenged by deoxyMb^{II} to give Mb^{II}(NO), which has a much stronger binding constant (K_{NO}= 1.4 × 10^{11} and 1.4 × 10^{4} M^{-1} for wt deoxyMb^{II} and wt metMb^{III}, respectively) [31, 44] and is not readily oxidized by aqueous NO_2^-. These processes are occurring in the present case as well and are responsible for the temporal decrease in absorbance first seen at the Soret band maximum of deoxyMb^{II} (433 nm). However, since the reaction illustrated by Fig. 8 was carried out with ferrous solutions generated by excess cysteine (designated as CysSH in Scheme 1), any metMb^{III} so formed is susceptible to further reduction, albeit more slowly. As a consequence, all of the deoxyMb^{II} is eventually converted to the nitrosyl complex Mb^{II}(NO). This sequence of events explains the shape of the temporal absorbance changes seen in Fig. 8, since the molar absorbance of deoxyMb^{II} at 433 nm is less than that of Mb^{II}(NO).

As noted above, the rate constants k_2 for the cysteine reduction of wt metMb^{III} and the analogous ferric mutant proteins were measured independently by following the absorbance decrease at the λ_{max} of the ferric derivatives in the absence of added nitrite. Since this step is slower than the nitrite reductase rates under the reaction conditions, and k_2' values for the NiR reactions indicated in Scheme 1 could be determined by monitoring the change in absorbance at the Soret band λ_{max} of deoxyMb^{II}. The second order rate constants in both cases were calculated from the initial rates as shown below. A single concentration of NO_2^- (1 mM) was used in these experiments; however, previous studies with hh Mb have shown the reaction rate to be linear in [NO_2^-] to 5 mM.[45]

$$k_2 = \frac{-(d[Mb^{III}]/dt)_{initial}}{[Mb^{III}]_{initial}[CysSH]} \quad k_2' = \frac{-(d[Mb^{II}]/dt)_{initial}}{[Mb^{II}]_{initial}[NO_2^-]}$$

A legitimate concern is whether excess cysteine affects the rate of nitrite reduction. In order to test this, the wt metMb^{III} was first reduced then the excess cysteine was removed from its solution with wt deoxyMb by passing the solution over a G-25 Sephadex column. The rates of nitrite reduction by the ferrous protein were then investigated as described above. Notably, we found no significant difference between the initial rates of the nitrite reduction reactions when excess cysteine was present (k_2' = 5.5 M^{-1} s^{-1}) and when it was absent (k_2' = 6.0 M^{-1} s^{-1}). The latter nitrite reduction rate obtained was similar to that obtained for dithionite-reduced wt deoxyMb^{II} (k_2' = 5.8 M^{-1}s^{-1}) obtained here and the previously reported value of 6 M^{-1}s^{-1} under analogous conditions.[45] Similar results were obtained for the two mutant proteins as well. It is also notable that we did not detect (using electrospray ionization mass spectrometry) any *S*-nitrosocysteine in the reaction mixture when excess cysteine was employed as the reductant. Nor could we detect any reaction between cysteine and free NO under our reaction conditions with 0.1 mM of the stronger metal chelator DTPA (diethylenetriamminepentaacetic acid), which was used to prevent Fe^{2+} and Cu^{2+} mediated decomposition of nitrosothiols.[46]

Fig. 8 illustrates the temporal absorbance changes at 433 nm occurring upon adding nitrite to a solution of wt deoxyMb^{II} and shows the two stages of the overall reaction as described above. The faster first stage (nitrite reduction) can be fit to an exponential function giving a k_{obs} value consistent with the rates determined by the initial rates method. However, the situation is different for the mutant proteins where the values of k_2[CysSH] and k_2'[NO_2^-] are more comparable under the reaction conditions, thus making it complicated to separate the two processes. For this reason, the nitrite reduction kinetics for each of these systems were analyzed

by the initial rates method, where the initial rates were calculated from the absorbance changes over the first 10% of the each reaction.

In this manner the second order rate constants (in units of $M^{-1}s^{-1}$) for the nitrite reduction of the wt and mutant proteins were determined to be wt (5.5) > H64V/V67R (1.8) > H64V (0.35) (the analogous experiments done in dithionite reduced, reductant-free solutions were 5.8, 1.6 and 0.29 M^{-1} s^{-1} for wt Mb, H64V/V67R, and H64V, respectively). The nitrite reduction activity of the H64V Mb^{II} mutant is only ~ $1/16^{th}$ that of wt Mb^{II}. This suggests that the weaker binding-/activation of the *N*-bound nitrite and/or the absence of a distal H-bonding residue slows the nitrite reduction by the ferrous myoglobin H64V mutants. Consistent with this view is the observation that nitrite reduction by the H64V/V67R double mutant is five-fold faster than that by the single H64V mutant, although still somewhat slower than that by the wt protein. The kinetics data for the second-order rate constants described in this section are summarized in Table 2.

Discussion

Nitrite Linkage Isomerism in Synthetic Heme Models

Both the nitro and nitrito binding modes shown in Fig. 1 have been determined crystallographically for metalloporphyrin nitrite complexes. The nitro binding mode is, with one exception, the only binding mode established to date for *both* ferric and ferrous porphyrins.[47–49] The exception is that for the $[(TpivPP)Fe(NO_2)(NO)]^-$ (TpivPP = tetra (pivalamidophenyl)porphyrinato dianion) complex that exhibits a 60:40 disorder of the $FeONO:FeNO_2$ binding modes in the same crystal.[48]

Without exception, the X-ray crystal structures of cobalt porphyrins complexed with nitrite reveal the *N*-binding mode of nitrite.[47, 50–53] However, laser flash photolysis of the nitro complex $(TPP)Co(NO_2)$ (TPP = tetraphenylporphyrinato dianion) in benzene results in photodissociation of the NO_2 ligand which recombines to give the metastable nitrito species (TPP)Co(ONO). A nitrito-to-nitro linkage isomerization occurs to regenerate the thermodynamically more stable nitro complex $(TPP)Co(NO_2)$.[54]

The nitrito binding mode has been the only one determined to date in crystal structures of nitrite adducts of synthetic metalloporphyrins of Mn,[55] Ru,[56–59] and Os.[60] Interestingly, however, flash photolysis of the (TPP)Mn(ONO) complex in toluene results in the dissociation of the nitrite ligand, and recombination follows second-order kinetics to generate the intermediate nitro complex $(TPP)Mn(NO_2)$, which then isomerizes to the stable nitrito species (TPP)Mn (ONO).[61]

Are the N-bound and O-bound nitrite linkage isomers close in energy in synthetic iron porphyrins?—Results from experimental investigations and theoretical calculations suggest this to be the case. The low temperature photolysis of the six-coordinate $(TPP)Fe(NO)(NO_2)$ complex as a KBr pellet results in IR spectral changes associated with a nitro-to-nitrito linkage isomerization process to yield the metastable (TPP)Fe(NO)(ONO) species.[62, 63] The existence of this metastable linkage isomer was confirmed by ^{15}N isotope-labeling experiments and by extensive DFT calculations on the model porphine system. The theoretical calculations on the model $(P)Fe(NO)(NO_2)$ compound predicted that the nitrito FeONO isomer was only ~4.3 kcal/mol higher in energy than the nitro $FeNO_2$ isomer. Such linkage isomerization was also observed during the reactions of the in situ generated (por)Fe (ONO) (por = TPP, TTP; TTP = tetratolylporphyrinato dianion) compounds with NO[64, 65] or NH_3;[66] the low temperature reactions gave the intermediate six-coordinate (por)Fe(L)(ONO) (por = TPP, TTP; L = NO, NH_3) compounds that underwent linkage isomerization upon warming to the thermodynamically more stable nitro (por)Fe(L)(NO_2) derivatives. DFT

calculations on the model (P)Fe(ONO) compound (P = porphinato dianion) predicted near-identical energies for the experimentally observed nitrito and the not-yet-observed nitro isomers.[64]

Related DFT theoretical calculations on the six-coordinate model compound (P)Fe(NO_2)(ImdH) reveal a thermodynamic preference for the nitro binding mode in these compounds by 4.5 kcal/mol in the ferric form and 6 kcal/mol in the ferrous form;67 similar energy differences of 5–10 kcal/mol, depending on the basis sets used, were obtained for the same system in a recent study.68 These results are not inconsistent with an earlier calculation on the model compound (P)Fe(NO_2)(NH_3) that showed a thermodynamic preference, by over 10 kcal/mol, for the nitro binding mode in the ferric form.[69]

Nitrite Linkage Isomerism in Heme Proteins

There were no reports of linkage isomerization involving nitrite ligands in any heme protein prior to our results presented in this article. The *N*-binding mode of nitrite has been observed in the crystal structures of the nitrite adducts of cyt cd_1 NiR from *P. pantotrophus*,[12] the sulfite reductase hemoprotein from *E. coli*,[70] and cyt *c* NiR from *W. succinogenes*.[69] This *N*-binding mode is retained in the nitrite adduct of the Y218F mutant of cyt *c* NiR that has a conserved and critical H-bonding (to nitrite) residue mutated to a non-H-bonding residue.[13]

Our determination of the *O*-binding mode of nitrite in crystals of hh Mb^{III}(ONO) was thus unexpected.[14] Importantly, this *O*-binding was the sole binding mode found when crystals of $metMb^{III}$ were soaked with nitrite, or when crystals of the product were grown from preformed Mb^{III}(ONO) in solution, indicating that this binding mode was not due to an artificial constraint of the distal pocket of preformed $metMb^{III}$ crystals. In this compound, the FeONO moiety was found in the classical *trans* conformation (Fig. 5). A similar *trans*-FeONO conformation was determined for the nitrite ligand in the Mn-substituted derivative Mn^{III}Mb(ONO).[71] In the case of the nitrite adduct of human tetrameric hemoglobin that also exhibits *O*-binding of nitrite, the FeONO moiety was found in the *trans* conformation in the α subunit, but was found in a distorted *cis*-like conformation in the β subunit.[15]

Our attempts to date at generating a Mb^{II}(ONO) complex have not been successful. For example, we have attempted to generate such a ferrous complex through (i) the stoichiometric addition of nitrite to ferrous deoxyMb^{II} crystals, and (ii) the addition of sub-stoichiometric to stoichiometric amounts of reducing agents to crystals of Mb^{III}(ONO).[14] In the case of the former attempts, it is known that nitrite will oxidize Mb^{II}s, and we observed this as well. In the case of the latter attempts, our crystal structural results showed a reduced occupancy of the nitrite in the distal pocket; not surprisingly, the nitrite occupancy was inversely related to the amount of reducing agent added, and the final structures obtained were those for the Mb^{II}NO compound.

We previously reported a different approach to gain insight into the possible *N*-binding mode of nitrite to Mb^{II}. As mentioned earlier, all crystal structures of cobalt porphyrins with nitrite ligands published to date display the *N*-binding mode of nitrite to the cobalt center. Furthermore, Co^{III}-substituted Mb is formally valence isoelectronic with Mb^{II}. Surprisingly, the crystal structure of the Co^{III}Mb(ONO) complex also reveals the *O*-binding mode of nitrite to the metal center.[71] This remains the only published report of *O*-binding of nitrite to any cobalt porphyrin, and clearly demonstrates the strong influence of the single H-bonding His64 residue in directing the *O*-binding of nitrite in Mbs.

Nitrite Binding to Mb Mutants

Given our observations described above, and given the fact that the calculated energy differences between the *N*-bonded and *O*-bonded forms of nitrite to hemes were on the order of H-bond stabilization energies, we hypothesized that the single His64 residue in Mb did indeed exert a strong influence in directing the *O*-binding mode of nitrite. Our crystal structure of the nitrite adduct of the Mb^{III} H64V single mutant, shown at the top of Fig. 3, confirms our hypothesis. Surprisingly, this is the first report of a change in nitrite conformation in any heme protein due to a mutation of a distal pocket residue, and is the first report of a variable coordination mode of nitrite in a heme protein. We also hypothesized that reintroducing a H-bonding residue into the distal pocket will restore the *O*-binding mode of nitrite to Mb^{III}. Our crystal structure of the nitrite adduct of the H64V/V67R double mutant, shown at the top of Fig. 4, also confirms this hypothesis. In this latter case, the *O*-bonded nitrite ligand is best modeled in a distorted *cis*-like conformation, rather than in the *trans* conformation observed in the wt Mb^{III}(ONO) structure.

Additional important clues on any preferential binding of nitrite to wt Mb^{III} are obtained from two recent computational studies. Basu et al. have reported that in a truncated Hb mono-subunit system containing the Fe-porphine, imidazole side chain H-bonded to an acetic acid group, and the distal His, the *N*-bonded nitro form was calculated to be more stable than the *O*-bonded nitrito form by ~7 kcal/mol.[72] Perissinotti et al. have similarly reported that for truncated subunits of Hb^{II}, the *N*-bound isomer of nitrite is favored over the *O*-bound form (by 9 kcal/mol for the α subunit, but by only 3 kcal/mol for the β subunit).[68] In the latter study, the authors concluded that both *N*- and *O*-bonded nitrite modes in the ferrous systems could contribute to NiR activity. This is consistent with an earlier proposal by Silaghi-Dumitrescu who suggested, based on DFT calculations, that both *N*- and *O*-bonded nitrite groups were catalytically competent in the related NiR activity of the ferrous cyt cd_1 NiR enzyme.[67]

It has been proposed that in both the Hb and cyt cd_1 NiR proteins, nitrite reduction can in principle occur by either of the energetically feasible *N*-bonded nitro or *O*-bonded nitrito modes.[67, 68] For the nitro mode, it still widely accepted that a formal double protonation of a nitro O-atom precedes the release of a H_2O molecule and the generation of a Fe^{III}-bound NO (structure I). In contrast, protonation of an *O*-bonded nitrito ligand would generate the ferric-hydroxo species and NO through an ON-O bond homolysis reaction (structure II).

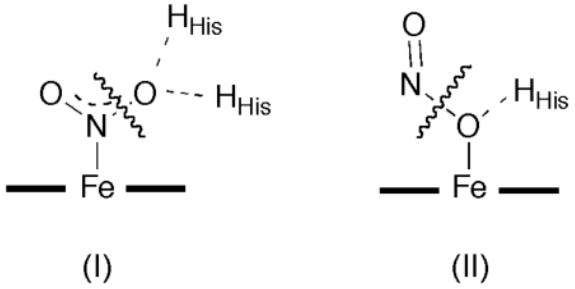

(I) (II)

Chemical precedent for the latter reaction has been provided for the reactions of alkyl nitrites with group 8 metalloporphyrins, in which NO is generated together with metal alkoxide products.[73–75]

As described in the Results section, the second order rate constants for nitrite reduction by the wt and mutant Mb^{II}s follow the order wt > H64V/V67R >> H64V. Given the calculated small energy differences between the *N*- and *O*-bonded modes of nitrite, we speculate that the presence of a distal H-bonding residue in the distal pocket is primarily responsible for this order. Thus, the double-mutant H64V/V67R is closest to the wt Mb protein in providing a

distal pocket H-bonding environment to the nitrite ligand, and this is reflected in a similar order of magnitude in the rate of nitrite reduction. In contrast, the nitrite ligand in its H64V adduct is missing this critical H-bonding residue. Indeed, the NiR activity of the H64V Mb^{II} mutant is only ~ $1/16^{th}$ that of wt Mb^{II}.

Summary

In this article, we demonstrate using site-directed mutagenesis that the single H-bonding distal pocket residue in hh Mb^{III} directs the bound nitrite anion towards the *O*-nitrito binding mode. Further, we have demonstrated the use of cysteine as a reducing agent for Mb^{III}s, and have shown that the NiR activity of the H64V Mb mutant lacking a distal H-bonding residue is markedly diminished, suggesting that the single His64 residue is a crucial factor in Mb-enabled nitrite reduction. We note that these results represent the first demonstration of a variation of nitrite binding mode as a function of distal pocket changes in a metalloprotein.

Acknowledgments

These studies were supported by the National Institutes of Health (GM076640; GBR-A) and the National Science Foundation (CHE-0749524, PCF). We thank Dr. Grant Mauk for the H64V plasmid, Dr. Mark Gladwin for helpful discussions on the related sperm whale Mb systems, Dr. Dany Kim-Shapiro for advice on removing adventitious dioxygen and Dr. Len Thomas for assistance with the crystallography.

References

1. Braida W, Ong SK. Water, Air, and Soil Pollution 2000;118:13–26.
2. Averill BA. Chem. Rev 1996;96:2951–2964. [PubMed: 11848847]
3. Eady, RR.; Hasnain, SS. Denitrification. In: Que, L., Jr; Tolman, WB., editors. Comprehensive Coordination Chemistry II. Vol. Vol. 8. San Diego, CA: Elsevier; 2004. p. 759-786.
4. Wasser IM, de Vries S, Moenne-Loccoz P, Schroder I, Karlin KD. Chem. Rev 2002;102:1201–1234. [PubMed: 11942794]
5. Tavares P, Pereira AS, Moura JJG. J. Inorg. Biochem 2006;100:2087–2100. [PubMed: 17070915]
6. Feelisch M, Fernandez BO, Bryan NS, Garcia-Saura MF, Bauer S, Whitlock DR, Ford PC, Janero DR, Rodriguez J, Ashrafian H. J. Biol. Chem 2008;283:33927–33934. [PubMed: 18835812]
7. Lundberg JO, Weitzbert E, Gladwin MT. Nat. Rev. Drug Disc 2008;7:156–167.
8. Alzawahra WF, Talukder MAH, Liu XP, Samouilov A, Zweier JL. Am. J. Physiol.-Heart Circ. Physiol 2008;295:H499–H508. [PubMed: 18539756]
9. Li HT, Cui HM, Kundu TK, Alzawahra W, Zweier JL. J. Biol. Chem 2008;283:17855–17863. [PubMed: 18424432]
10. Cosby K, Partovi KS, Crawford JH, Patel RP, Reiter CD, Martyr S, Yang BK, Waclawiw MA, Zalos G, Xu X, Huang KT, Shields M, Kim-Shapiro DB, Schechter AN, Cannon RO III, Gladwin MT. Nat. Med 2003;9:1498–1505. [PubMed: 14595407]
11. Hendgen-Cotta UB, Merx MW, Shiva S, Schmitz J, Becher S, Klare JP, Steinhoff HJ, Goedecke A, Schrader J, Gladwin MT, Kelm M, Rassaf T. Proc. Natl. Acad. Sci. USA 2008;105:10256–10261. [PubMed: 18632562]
12. Williams PA, Fulop V, Garman EF, Saunders NFW, Ferguson SJ, Hajdu J. Nature 1997;389:406–412. [PubMed: 9311786]
13. Lukat P, Rudolf M, Stach P, Messerschmidt A, Kroneck PMH, Simon J, Einsle O. Biochemistry 2008;47:2080–2086. [PubMed: 18201106]
14. Copeland DM, Soares A, West AH, Richter-Addo GB. J. Inorg. Biochem 2006;100:1413–1425. [PubMed: 16777231]
15. Yi J, Safo MK, Richter-Addo GB. Biochemistry 2008;47:8247–8249. [PubMed: 18630930]
16. Barrett ML, Harris RL, Antonyuk S, Hough MA, Ellis MJ, Sawers G, Eady RR, Hasnain SS. Biochemistry 2004;43:16311–16319. [PubMed: 15610025]

17. Antonyuk SV, Strange RW, Sawers G, Eady RR, Hasnain SS. Proc. Natl. Acad. Sci. U.S.A 2005;102:12041–12046. [PubMed: 16093314]
18. Guillemette JG, Matsushima-Hibiya Y, Atkinson T, Smith M. protein Eng 1991;4:585–592. [PubMed: 1891466]
19. Pflugrath J. Acta Cryst 1999;D55:1718–1725.
20. McCoy AJ, Grosse-Kunstleve RW, Adams PD, Winn MD, Storoni LC, Read RJ. J. Appl. Cryst 2007;40:658–674. [PubMed: 19461840]
21. Murshudov GN, Vagin AA, Dodson EJ. Acta Cryst 1997;D53:240–255.
22. Bailey S. Acta Cryst 1994;D50:760–763.
23. Emsley P, Cowtan K. Acta Cryst. D 2004;D60:2126–2132. [PubMed: 15572765]
24. Perrakis A, Morris R, Lamzin VS. Nat. Struct. Biol 1999;6:458–463. [PubMed: 10331874]
25. Arendall WB III, Tempel W, Richardson JS, Zhou W, Wang S, Davis IW, Liu Z-J, Rose JP, Carson WM, Luo M, Richardson DC, Wang B-C. J. Struct. Funct. Genomics 2005;6:1–11. [PubMed: 15965733]
26. DeLano, WL. The PyMOL Molecular Graphics System. San Carlos, CA, U.S.A: DeLano Scientific LLC; http://www.pymol.org
27. Laskowski RA, MacArthur MW, Moss DS, Thornton JM. J. Appl. Cryst 1993;26:283–291.
28. Stanier RY, Ingraham JL. J. Biol. Chem 1954;210:799–808. [PubMed: 13211618]
29. Sono M, Dawson JH. J. Biol. Chem 1982;257:5496–5502. and references therein. [PubMed: 6279603]
30. Springer BA, Sligar SG, Olson JS, Phillips GN Jr. Chem. Rev 1994;94:699–714.
31. Olson JS, Phillips GN Jr. J. Biol. Chem 1996;271:17593–17596. [PubMed: 8698688]
32. Engler N, Prusakov V, Ostermann A, Parak FG. Eur. Biophys. J 2003;31:595–607. [PubMed: 12582819]
33. Quillin ML, Arduini RM, Olson JS, Philips GN Jr. J. Mol. Biol 1993;234:140–155. [PubMed: 8230194]
34. Conti E, Moser C, Rizzi M, Mattevi A, Lionetti C, Coda A, Ascenzi P, Brunori M, Bolognesi M. J. Mol. Biol 1993;233:498–508. [PubMed: 8411158]
35. Møller JKS, Skibsted LH. Chem. Rev 2002;102:1167–1178. [PubMed: 11942791]
36. Arnold EV, Bohle DS. Methods Enzymol 1996;269:41–55. [PubMed: 8791636]
37. Cox RP, Hollaway MR. Eur. J. Biochem 1977;74:575–587. [PubMed: 856586]
38. Nakamura M, Nakamura S. Biochim. Biophys. Acta 1996;1289:329–335. [PubMed: 8620016]
39. Antonini, E.; Brunori, M. Hemoglobin and Myoglobin In Their Reactions With Ligands. Vol. Vol. 21. North-Holland: Amsterdam; 1971.
40. Di Iorio EE. Methods Enzymol 1981;76:57–72. [PubMed: 7329277]
41. Millis KK, Weaver KH, Rabenstein DL. J. Org. Chem 1993;58:4144–4146.
42. Raven EL, Mauk AG. Adv. Inorg. Chem 2001;51:1–49.
43. Laverman LE, Wanat A, Oszajca J, Stochel G, Ford PC, van Eldik R. J. Am. Chem. Soc 2001;123:285–293. [PubMed: 11456515]
44. Hoshino M, Ozawa K, Seki H, Ford PC. J. Am. Chem. Soc 1993;115:9568–9575.
45. (a) Huang Z, Shiva S, Kim-Shapiro DB, Patel RP, Ringwood LA, Irby CE, Huang KT, Ho C, Hogg N, Schechter AN, Gladwin MT. J. Clin. Invest 2005;115:2099–2107. [PubMed: 16041407] (b) Shiva S, Huang Z, Grubina R, Sun J, Ringwood LA, MacArthur PH, Xu X, Murphy E, Darley, Usmar VM, Gladwin MT. Circ. Res 2007;100:654–661. [PubMed: 17293481]
46. McAninly J, Williams DLH, Askew SC, Butler AR, Russell C. J. Chem. Soc., Chem. Commun 1993:1758–1759.
47. Wyllie GRA, Scheidt WR. Chem. Rev 2002;102:1067–1089. [PubMed: 11942787]
48. Nasri H, Ellison MK, Chen S, Huynh BH, Scheidt WR. J. Am. Chem. Soc 1997;119:6274–6283.
49. Nasri H, Ellison MK, Shang M, Schultz CE, Scheidt WR. Inorg. Chem 2004;43:2932–2942. [PubMed: 15106981]
50. Adachi H, Suzuki H, Miyazaki Y, Iimura Y, Hoshino M. Inorg. Chem 2002;41:2518–2524. [PubMed: 11978120]

51. Jene PG, Ibers JA. Inorg. Chem 2000;39:3823–3827. [PubMed: 11196776]
52. Yamamoto K, Iitaka Y. Chem. Lett 1989:697–698.
53. Goodwin J, Kurtikyan T, Standard J, Walsh R, Zheng B, Parmley D, Howard J, Green S, Mardyukov A, Przybla DE. Inorg. Chem 2005;44:2215–2223. [PubMed: 15792456]
54. Seki H, Okada K, Iimura Y, Hoshino M. J. Phys. Chem. A 1997;101:8174–8178.
55. Suslick KS, Watson RA. Inorg. Chem 1991;30:912–919.
56. Kadish KM, Adamian VA, Caemelbecke EV, Tan Z, Tagliatesta P, Bianco P, Boschi T, Yi G-B, Khan MA, Richter-Addo GB. Inorg. Chem 1996;35:1343–1348. [PubMed: 11666330]
57. Miranda KM, Bu X, Lorkovic I, Ford PC. Inorg. Chem 1997;36:4838–4848. [PubMed: 11670164]
58. Bohle DS, Hung C-H, Smith BD. Inorg. Chem 1998;37:5798–5806.
59. Lim MH, Lippard SJ. Inorg. Chem 2004;43:6366–6370. [PubMed: 15446885]
60. Leal FA, Lorkovic IM, Ford PC, Lee J, Chen L, Torres L, Khan MA, Richter-Addo GB. Can. J. Chem 2003;81:872–881.
61. Hoshino M, Nagashima Y, Seki H, Leo MD, Ford PC. Inorg. Chem 1998;37:2464–2469.
62. Lee J, Kovalevsky AY, Novozhilova IV, Bagley KA, Coppens P, Richter-Addo GB. J. Am. Chem. Soc 2004;126:7180–7181. [PubMed: 15186147]
63. Novozhilova IV, Coppens P, Lee J, Richter-Addo GB, Bagley KA. J. Am. Chem. Soc 2006;128:2093–2104. [PubMed: 16464112]
64. Kurtikyan TS, Hovhannisyan AA, Hakobyan ME, Patterson JC, Iretskii A, Ford PC. J. Am. Chem. Soc 2007;129:3576–3585. [PubMed: 17338521]
65. Kurtikyan TS, Ford PC. Angew. Chem. Int. Ed 2006;45:492–496.
66. Kurtikyan TS, Hovhannisyan AA, Gulyan GM, Ford PC. Inorg. Chem 2007;46:7024–7031. [PubMed: 17636900]
67. Silaghi-Dumitrescu R. Inorg. Chem 2004;43:3715–3718. [PubMed: 15180427]
68. Perissinotti LL, Marti MA, Doctorovich F, Luque FJ, Estrin DA. Biochemistry 2008;47:9793–9802. [PubMed: 18717599]
69. Einsle O, Messerschmidt A, Huber R, Kroneck PMH, Neese F. J. Am. Chem. Soc 2002;124:11737–11745. [PubMed: 12296741]
70. Crane BR, Siegel LM, Getzoff ED. Biochemistry 1997;36:12120–12137. [PubMed: 9315849]
71. Zahran ZN, Chooback L, Copeland DM, West AH, Richter-Addo GB. J. Inorg. Biochem 2008;102:216–233. [PubMed: 17905436]
72. Basu S, Grubina R, Huang J, Conradie J, Huang Z, Jeffers A, Jiang A, He X, Azarov I, Seibert R, Mehta A, Patel R, King SB, Hogg N, Ghosh A, Gladwin MT, Kim-Shapiro DB. Nat. Chem. Biol 2007;3:785–794. [PubMed: 17982448]
73. Richter-Addo GB. Acc. Chem. Res 1999;32:529–536.
74. Yi G-B, Chen L, Khan MA, Richter-Addo GB. Inorg. Chem 1997;36:3876–3885.
75. Andreasen LV, Lorkovic IM, Richter-Addo GB, Ford PC. Nitric Oxide: Biology and Chemistry 2002;6:228–235.

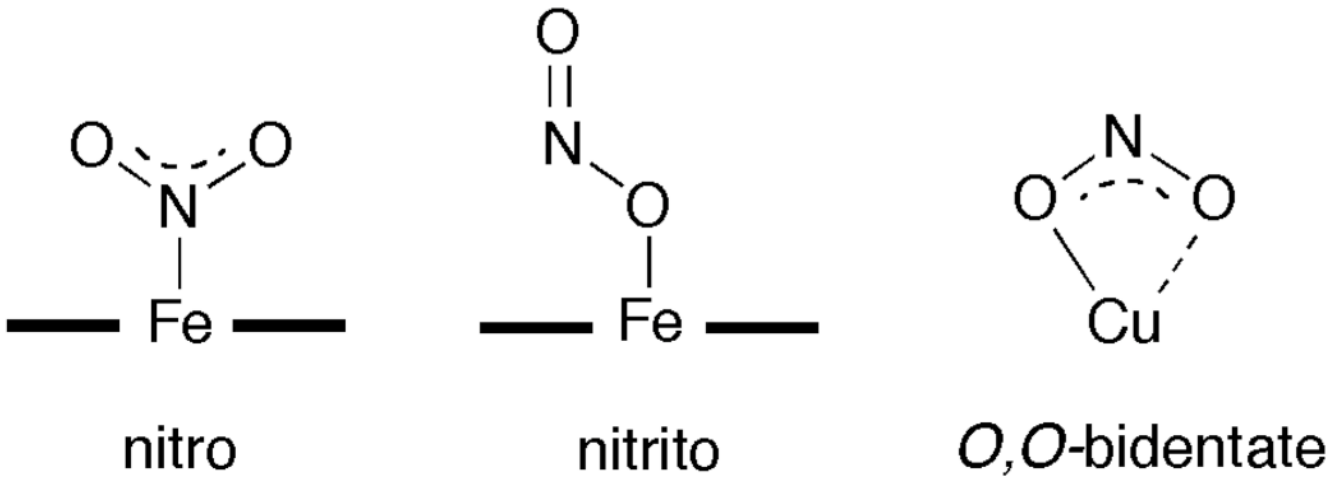

Figure 1.
Crystallographically determined binding modes of nitrite to heme proteins and copper enzymes.

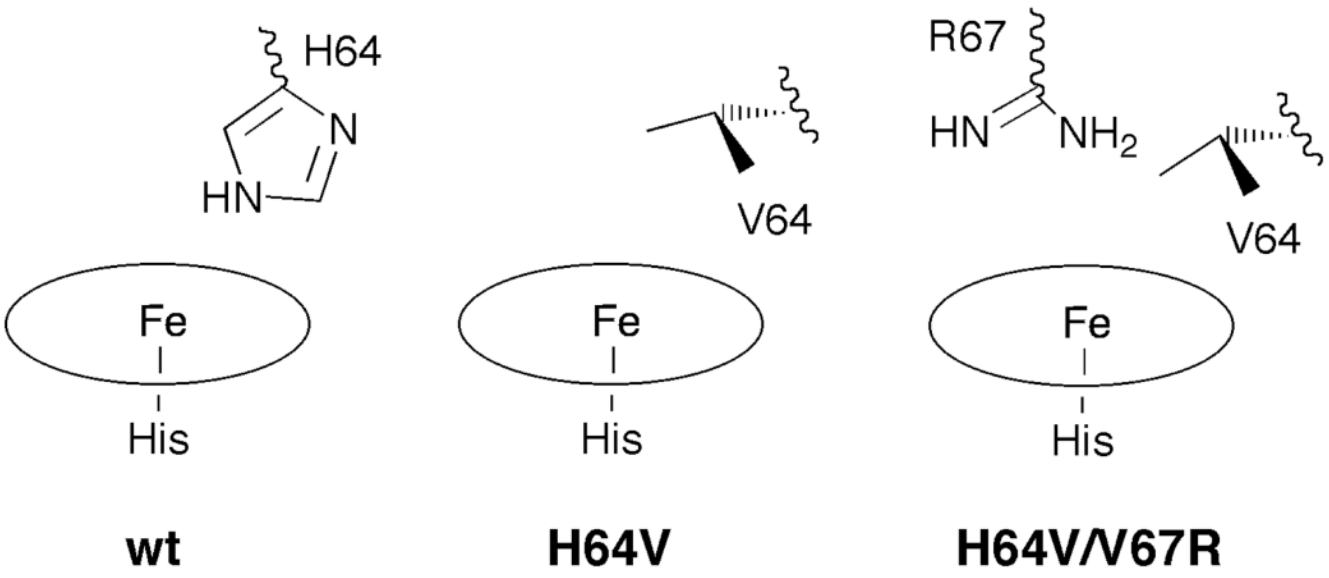

Figure 2.
Sketches of the active sites of wild-type (wt) and mutant Mbs.

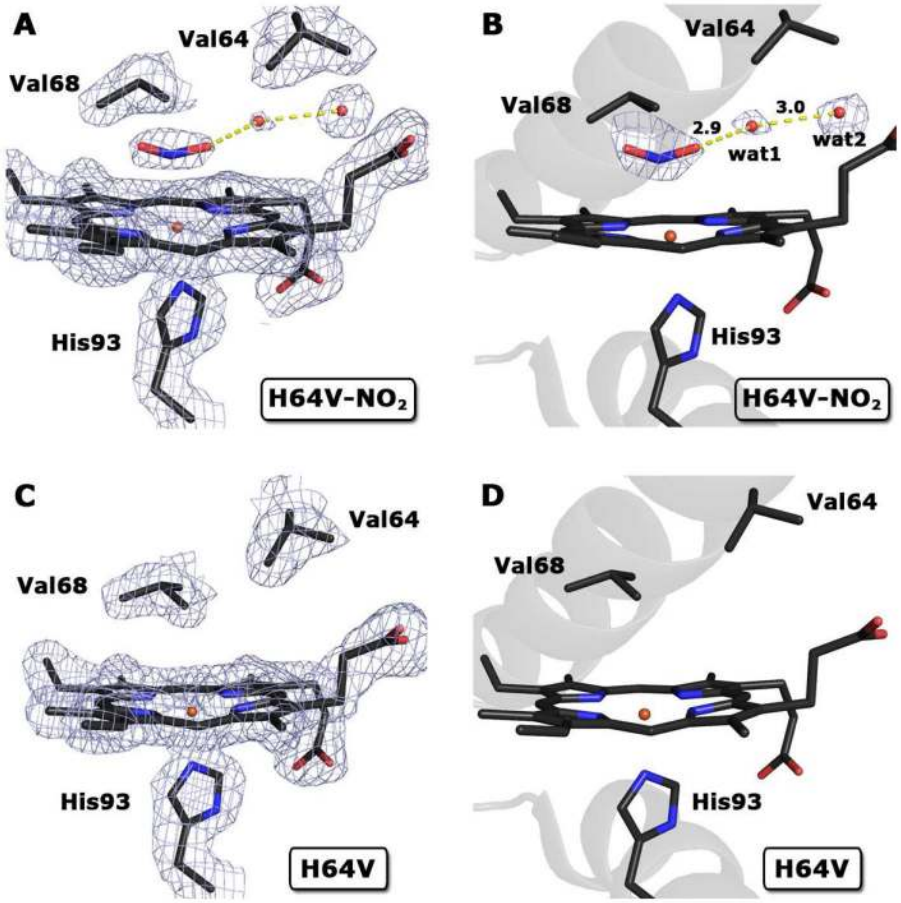

Figure 3.

The $2F_o-F_c$ electron density maps (left; contoured at 1σ) and F_o-F_c electron density map (right; contoured at 3σ) and final models of the heme environments in the crystal structures of the ferric hh Mb H64V single mutant. The 1.95 Å resolution crystal structure of the nitrite adduct of this H64V mutant is shown in **A** and **B** (PDB access code 3HEP). The 2.0 Å resolution crystal structure of the ferric H64V mutant without nitrite is shown in **C** and **D** (PDB access code 3HC9).

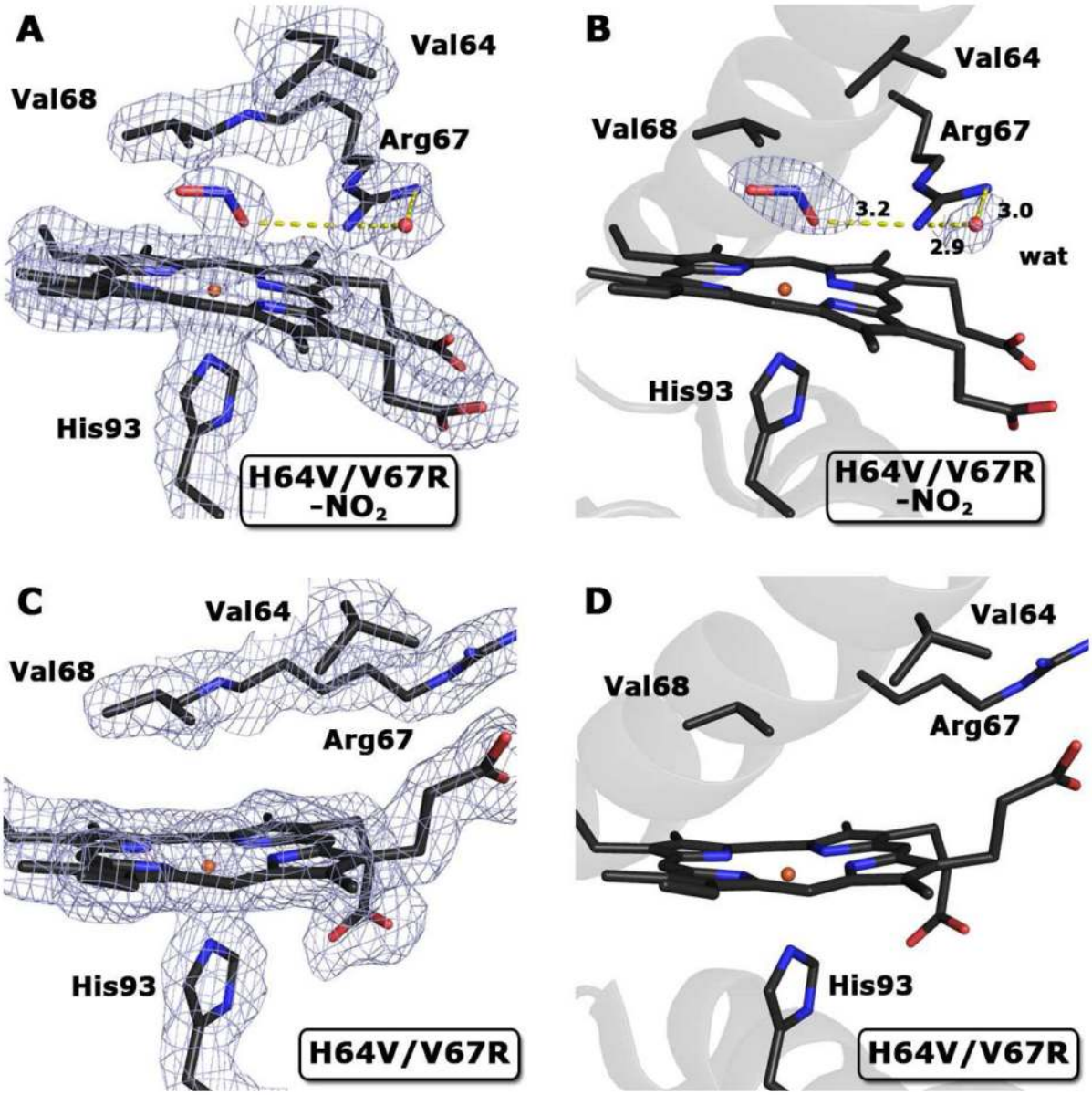

Figure 4.

The $2F_o-F_c$ electron density maps (left; contoured at 1σ) and F_o-F_c electron density map (right; contoured at 3σ) and final models of the heme environments in the crystal structures of the ferric hh Mb H64V/V67R double mutant. The 2.0 Å resolution crystal structure of the nitrite adduct of this H64V/V67R mutant is shown in **A** and **B** (PDB access code 3HEO). The 1.90 Å resolution crystal structure of the ferric H64V/V67R double mutant without nitrite is shown in **C** and **D** (PDB access code 3HEN).

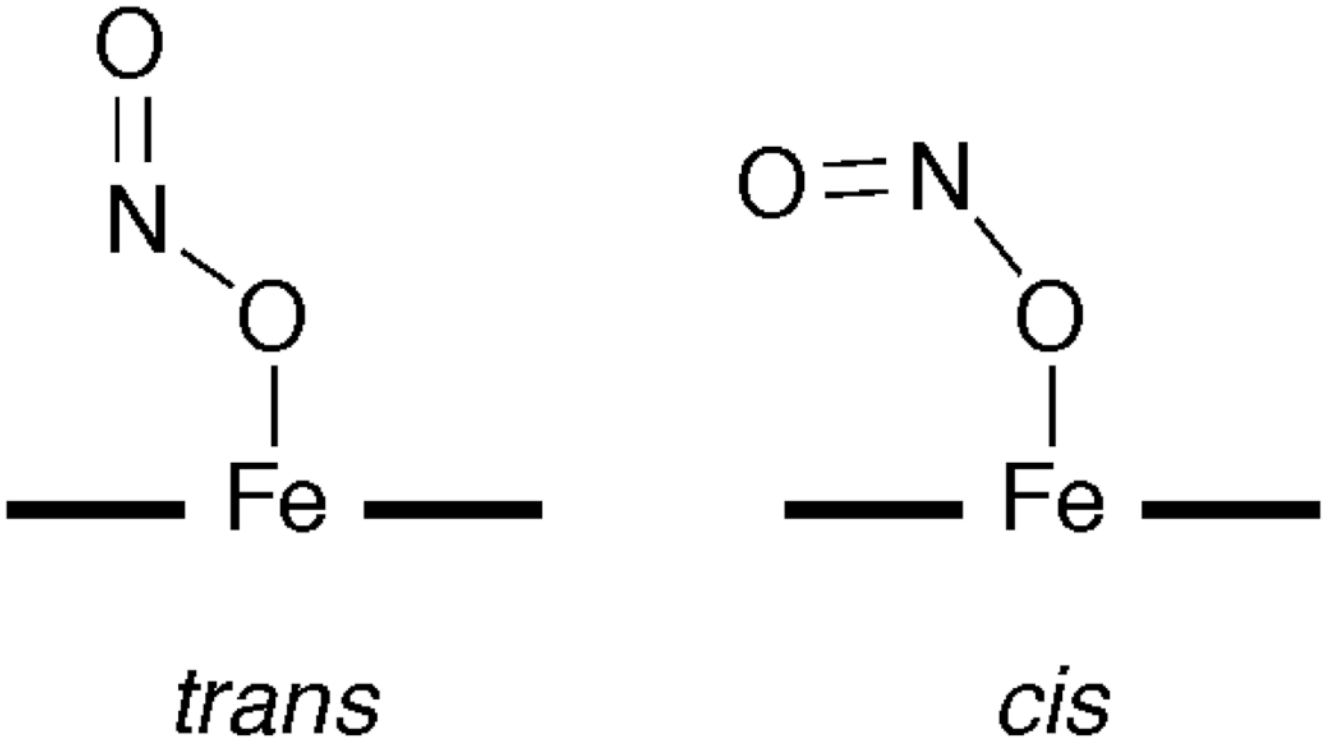

Figure 5.
The *trans*-FeONO and *cis*-FeONO conformations.

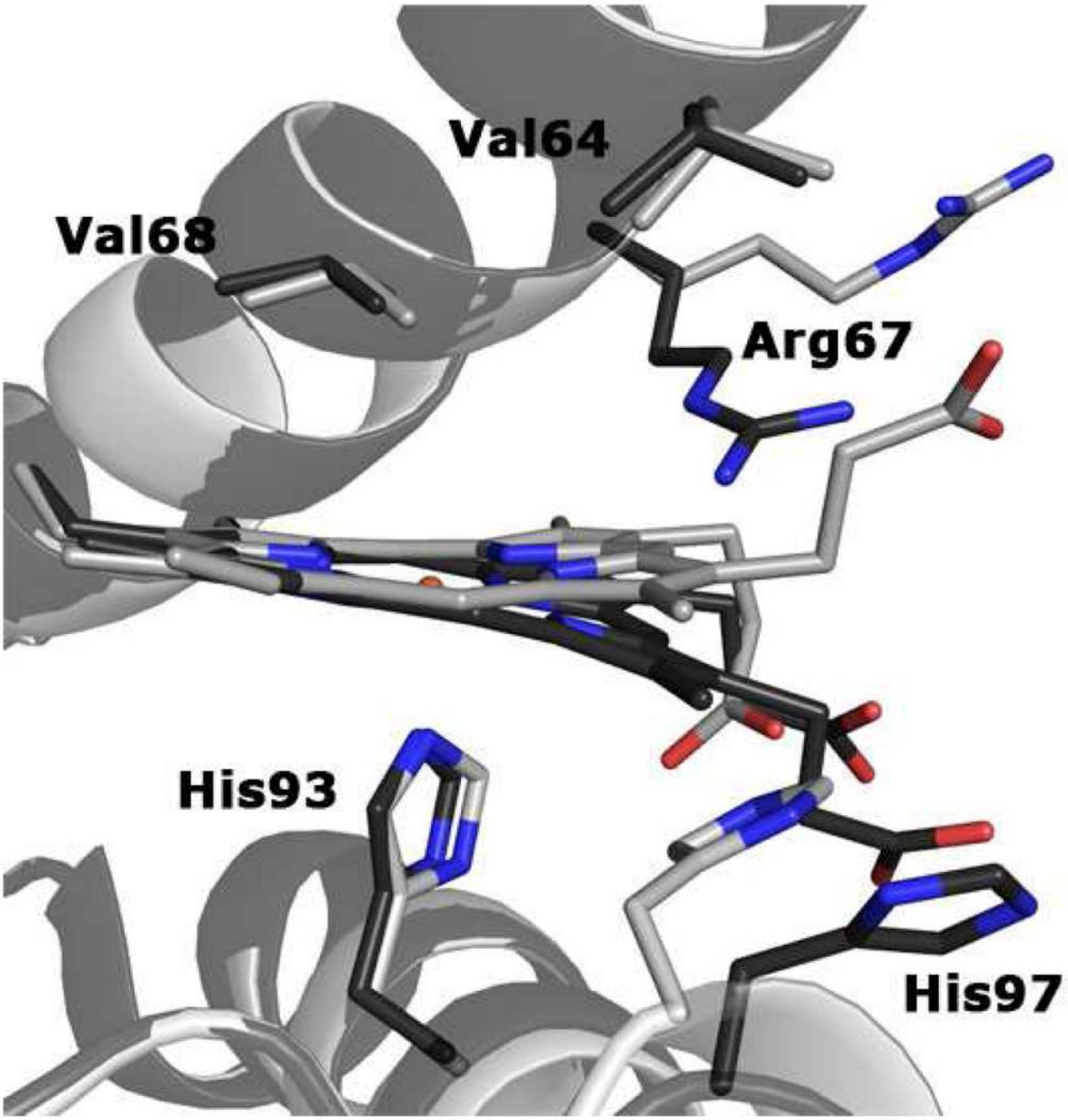

Figure 6.
Superposition of the final models of the active sites of the ferric hh Mb H64V/V67R (light gray) and that of the ferric hh Mb H64V/V67R-nitrite complex (dark gray) structures. The nitrite ligand is not shown.

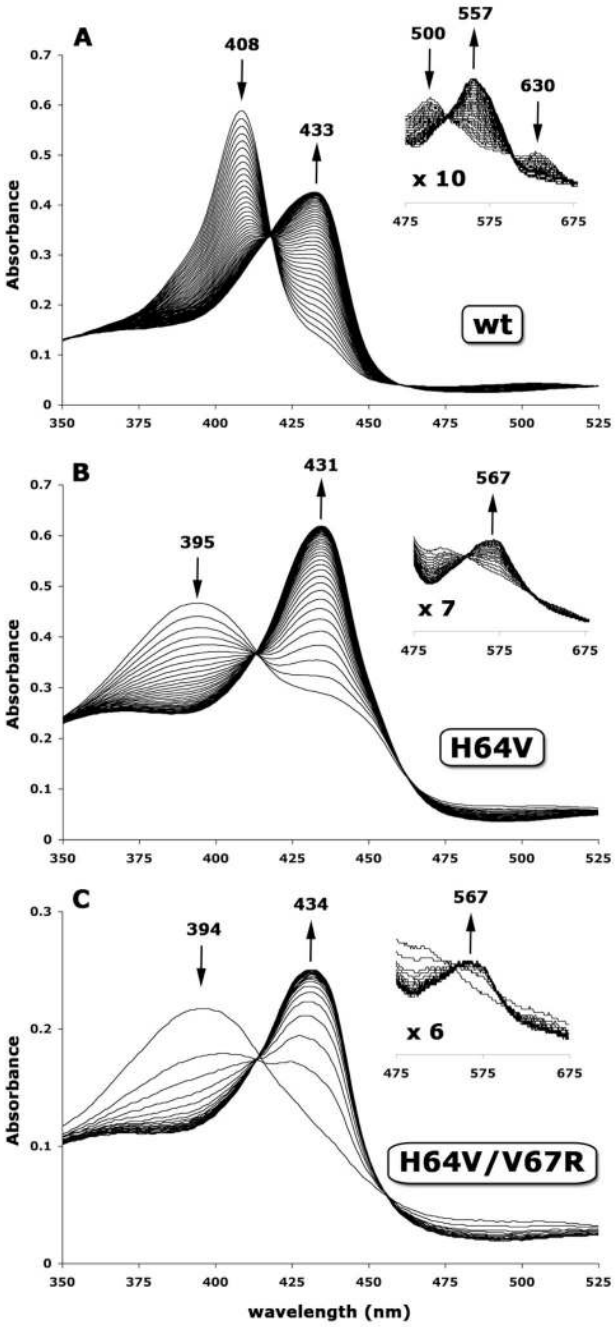

Figure 7.

UV-vis spectroscopic monitoring of the reactions of the metMbs with excess cysteine (1 mM) under anaerobic conditions in 0.1 M phosphate buffer at pH 7.41 at 25 °C. **A**: [wt] = 3.7 μM. **B**: [H64V] = 3.7 μM. C: [H64V/V67R] = 3.5 μM.

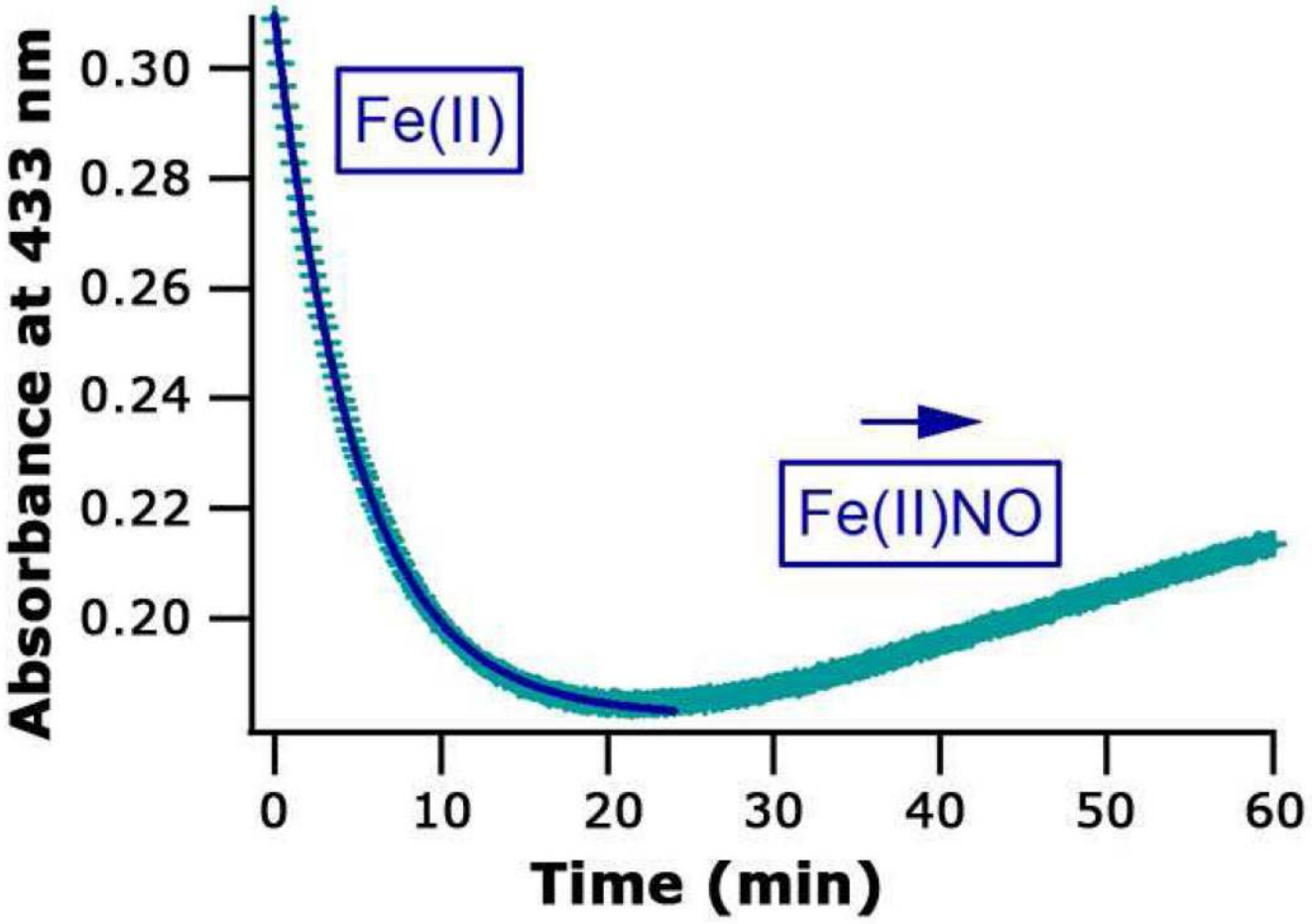

Figure 8.

The reaction between cysteine reduced wt Mb^{II} (2.5 μM) and nitrite (1 mM) was monitored by UV/vis at 25 °C in 0.1 M phosphate buffer at pH 7.41. The loss in absorbance for Fe^{II} at 433 nm was used to calculate the initial rates. After Fe^{II} oxidation in excess cysteine the reaction proceeds to form $Fe^{II}(NO)$ on the same timescale as the rate limiting cysteine reduction.

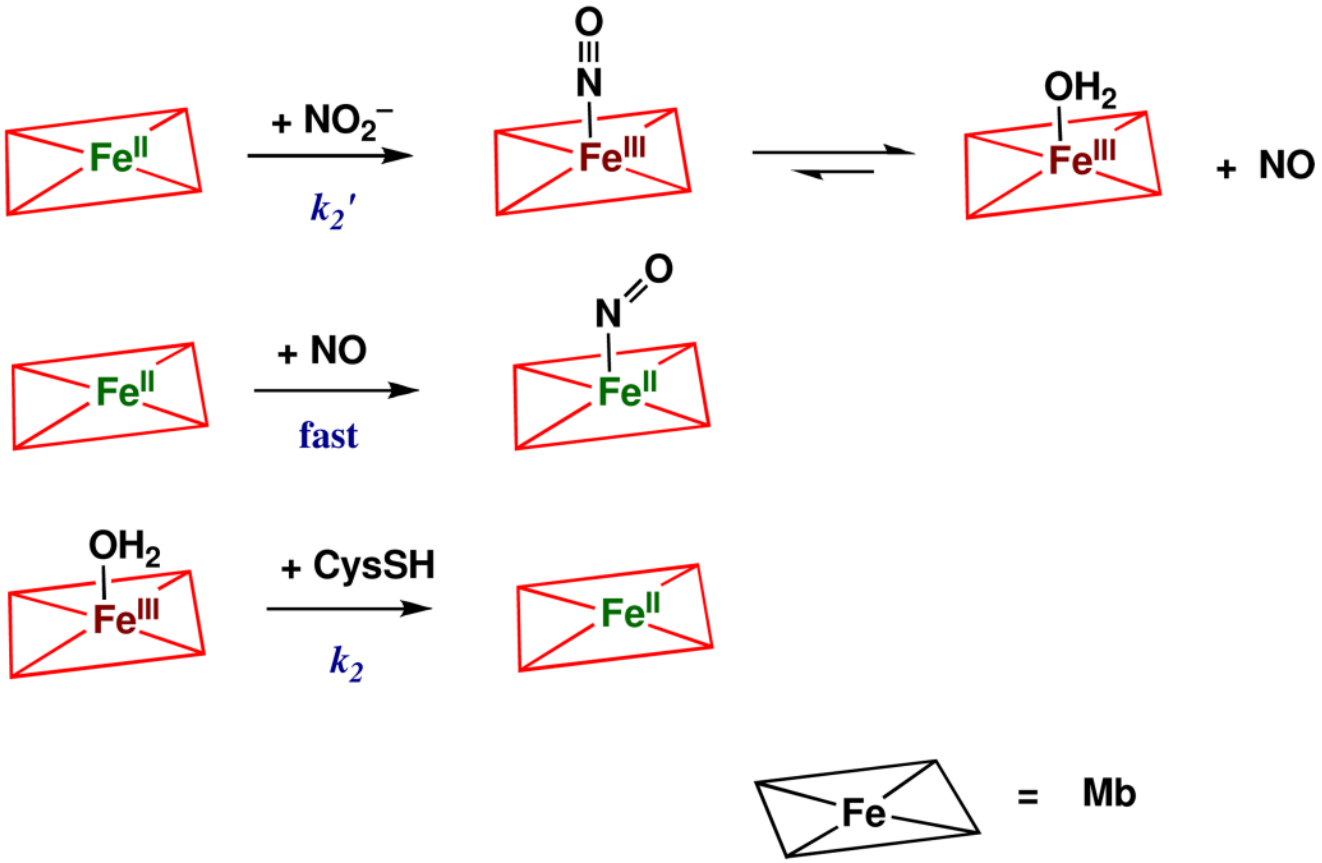

Scheme 1.

Table 1

X-ray data collection and refinement statistics

	H64V Mb^{III}	H64V Mb^{III} nitrite	H64V/V67R Mb^{III}	H64V/V67R Mb^{III} nitrite
PDB access code	3HC9	3HEP	3HEN	3HEO
A. Crystal parameters				
Space Group	$P2_12_12$	$P2_12_12$	$P2_12_12$	$P2_12_12$
Unit cell dimensions				
a, *b*, *c* (Å)	30.64, 119.24, 56.68	30.39, 119.39, 57.15	30.32, 119.00, 56.78	29.84, 118.05, 57.36
α, β, γ (°)	90.0, 90.0, 90.0	90.0, 90.0, 90.0	90.0, 90.0, 90.0	90.0, 90.0, 90.0
Solvent content (%)	54.07	54.24	54.35	53.83
B. Data collection				
Wavelength (Å)	1.5418	1.5418	1.5418	1.5418
Temperature (K)	104	100	104	100
Resolution range (Å)	20.8-2.0	23.2-1.95	24.4-1.9	20.6-2.0
Number of observations	109483	110170	108894	98292
Unique reflections	15752	15767	15394	13595
Multiplicity	7.42(7.44)	6.99(7.07)	7.07(7.32)	7.23(7.17)
Completeness (%)	100(100)	100(99.1)	91.0(91.5)	93.9(91.0)
Mean *I/σ(I)*	9.4(2.9)	7.1(2.8)	11.0(3.3)	9.9(3.3)
R_{merge} (%)[b]	9.8(49.0)	12.5(50.3)	7.6(46.2)	9.6(57.1)
C. Refinement				
Resolution (Å)	2.0	1.95	1.90	2.0
Number of protein atoms	1239	1239	1243	1243
Number of heteroatoms	118	128	158	101
R-factor (%)[c]	18.6	19.8	18.0	20.2
R_{free} (%)[d]	23.7	25.0	23.3	25.8
Average B-factors ($Å^2$)	27.2	26.6	27.7	29.9
R.m.s.d. from standard geometry				
Bond lengths (Å)	0.028	0.028	0.024	0.027
Bond angles (°)	2.10	2.09	1.92	2.13
Ramachandran plot (%)[e]				
Most favored region	96.03	94.04	95.24	94.7
Allowed region	3.97	5.96	4.76	5.3
Disallowed region	0	0	0	0

[a] The data in brackets refer to the highest resolution shell.

[b] $R_{merge} = \Sigma| I - \langle I \rangle ||/\Sigma(I)$ Where *I* is the individual intensity observation and $\langle I \rangle$ is the mean of all measurements of *I*.

[c] $R = \Sigma||F_O| - |F_C||/\Sigma|F_O|$ where F_O and F_C are the observed and calculated structure factors, respectively.

[d] R_{free} was calculated using 5% of the randomly selected diffraction data which were excluded from the refinement.

[e] As calculated using PROCHECK.[27]

Table 2

Second order rate constants (25 °C) for the anaerobic reduction of the metMb^{III}s and anaerobic nitrite reduction by the Mb^{II}s.

	Mb^{III} plus cysteine	Mb^{II} plus nitrite
	k_2($M^{-1}s^{-1}$)	k_2' ($M^{-1}s^{-1}$)
wt	0.069	5.5
H64V	0.60	0.35
H64V/V67R	2.3	1.8